Dynamics of Solvation in Supercritical Water

Mario Re and Daniel Laria*

Unidad de Actividad Química, Comisión Nacional de Energía Atómica, Avenida del Libertador 8250, 1429 Capital Federal, Argentina, and INQUIMAE, Facultad de Ciencias Exactas y Naturales, Universidad de Buenos Aires, Ciudad Universitaria, Pabellón II, 1428 Capital Federal, Argentina

Received: May 21, 1997; In Final Form: September 9, 1997[⊗]

Dynamical aspects of the dielectric response of supercritical water following an instantaneous charge jump on an initially neutral Lennard-Jones solute are investigated using molecular dynamics. The SPC model was used to describe solvent−solvent interactions. The simulation experiments were performed over the density interval spanning from 0.3 up to 1 g cm^{-3} along the 645 K isotherm. Compared to room temperature results, the overall solvation process at high densities is an order of magnitude faster and becomes progressively slower as we move toward lower densities. In all cases, the nonequilibrium solvent responses present a bimodal behavior characterized by a fast inertial regime lasting a few femtoseconds followed by a much slower diffusional regime that dominates the long time behavior. This last portion of the response, which contributes to a small extent at high densities, accounts for the major contribution at lower densities. Predictions from linear response theory are quite accurate at high densities and become less adequate at lower densities. Instantaneous normal-mode analysis of the dynamics of the pure solvent and of the early stages of solvation are also performed; rotational modes provide the major contribution to the short time dynamics of the response at all densities.

1. Introduction

In recent years, the subject of chemical reactivity in supercritical media has attracted increasing attention due to its important technological applications. Many processes such as, for example, selective fluid extraction and transport of matter or supercritical water oxidation for safe disposal of hazardous organic wastes, make successful use of the special properties exhibited by many solvents above or in the close vicinity of their critical points.[1−3] Two key ingredients combine to make chemical reactivity in supercritical media so peculiar. The first one is the high compressibility of the solvent allowing large variations of the bulk density via relatively minor changes in the applied pressure. This characteristic has profound effects on solubility parameters[4] and transport properties that lead to displacements of chemical equilibria[5] and substantial modifications in the kinetics of the reactive processes.[6] Moreover, the high suceptibility is clearly manifested in the large values of the measured partial molar volumes of solutes[7] and also explains the strong fluctuations of the local solvent density fields around attractive solutes.[8] The second important aspect is related to changes in the solvent polarity, most notably reflected in the magnitude of the bulk dielectric constant; the drop of ϵ to a value close to 6 at near-critical conditions transforms water into an "organic-like" environment where nonpolar solutes become even more soluble than ionic species.

Of course, one can trace the origins of many of the above-mentioned features back to modifications in the fluid structure that take place at molecular level. Returning to the specific case of water, the changes in the dielectric behavior are normally attributed to the gradual reduction of the hydrogen bonding as the temperature is raised. However, this rather intuitive assertion is still subjected to debate due to some discrepancies found in the intramolecular spatial correlations computed by different approaches. On one hand, recent neutron-scattering experiments[9] and ab initio molecular dynamics calculations[10] show a drastic reduction of the first peak of the oxygen−hydrogen radial distribution function at 573 K, reaching a complete disappearance at 673 K. On the other hand, results from infrared absorption[11] and proton NMR chemical shift[12] along with computer simulation studies using effective, mean field pseudopotentials would seem to indicate the persistence of a nonnegligible extent of hydrogen bonding even in supercritical states with densities as low as one-tenth of the standard room-temperature value.[13−18] Although not totally conclusive, a recent critical analysis of the available neutron diffraction data[19] would suggest that a plausible explanation to account for part of these discrepancies could be found in some inadequacies of the mean field effective Hamiltonians employed in the simulation studies.[20]

The previous paragraphs have clearly underlined the importance of solvation affecting equilibrium and kinetical aspects of reactive processes taking place at supercritical conditions. Focusing now our attention on the specific case of aqueous solutions, theoretical studies of solvation at extreme conditions have been exclusively directed to compute equilibrium properties, basically solvation free energies. For example, based on the classic expression of Born, a continuum model has been developed by Wood et al.[21] to incorporate effects of electrostriction in the computation of chemical potentials of aqueous electrolytes at high temperatures. With a similar spirit, Luo et al.[22] have implemented a method to explain the strong pressure dependence of the activation free energy for the hydrolysis of anisole in supercritical water. On the other hand, simulation studies have also been conducted to investigate the nature of potential of mean force between ion pairs[23] and to compute activation free energies for S_N2 reactions.[24]

Yet, equilibrium free energies do not provide the full picture. In reactions involving a substantial rearrangement of the electronic structure of the solute, the dynamical response of the medium plays a crucial role in affecting the kinetics of the processes.[25] At present, the dynamical characteristics of polar solvation at normal liquid conditions, i.e., not too far from the triple point, are sufficiently well established; a large body of

[⊗] Abstract published in *Advance ACS Abstracts,* November 1, 1997.

S1089-5647(97)01691-X CCC: $14.00

experimental research, analytical theories, and computer simulations has unveiled the main mechanisms through which the solvent is able to relax the excess of energy originally deposited on a given solute molecule.[26] The temporal characteristics of the solvation are usually determined in subpicosecond experiments via the determination of the time-dependent Stokes shift of the fluorescense spectrum of a chromophore.[29−32] Unfortunately, the time scales involved in the relaxation of aqueous solutions—normally estimated in the order of a few tens of femtoseconds—pose serious problems to direct experimental measurements due to restrictions in the time resolution available at this moment. Under these circumstances, simulation experiments remain as perhaps the most valuable tool with reliable predictive power.[33−49]

In an attempt to establish a connection with previous simulation experiments performed at ambient conditions,[34] the present paper examines dynamical aspects of aqueous solvation in supercritical aqueous environments; to be able to distinguish temperature from density effects, we have considered three well differentiated supercritical states spanning from liquidlike down to near-critical conditions. Of course the description presented here is far from being complete, and no efforts have been made at this point to mimic any particular reactive processes. Instead, we have concentrated in the characteristics of the dynamical response of a simple model for water following the instantaneous ionization of an originally neutral spherical solute. Following as closely as possible the actual experimental conditions, we have performed nonequilibrium simulations that monitored the time relaxation of the solute−solvent coupling; in addition, we explored the performance of linear response theory and a recently developed approach based on a harmonic approximation for the solvent dynamics, as well.

The remainder of this article is organized as follows: In section 2 we provide details of the model and methodology employed. Results from nonequilibrium simulation experiments are presented in section 3. Section 4 includes predictions of linear response theory, and in section 5 we consider the instantaneous normal-mode analysis of the solvation response. The concluding remarks are presented in section 6.

2. Model and Simulation Method

Our simulation experiments were performed on a system containing a solute particle and $N_w = 124$ water molecules. The three-site SPC model of Berendsen et al.[50] was used to describe water intermolecular interactions; the potential energy V_s for the solvent particles was considered as sum of pair contributions

$$V_s = \sum_{i<j}^{N_w} v(i,j) \tag{1}$$

The potential $v(i,j)$ between the ith and jth water molecules has a Lennard-Jones term between the oxygen sites and a sum of Coulomb terms due to the interactions between partial charges embedded at the oxygen and hydrogen sites

$$v(i,j) = v^{lj}(|\mathbf{r}_i^o - \mathbf{r}_j^o|) + \sum_{\alpha\gamma} v_{\alpha\gamma}^{coul}(|\mathbf{r}_i^\alpha - \mathbf{r}_j^\gamma|) \tag{2}$$

$$v^{lj}(r) = 4\epsilon[(\sigma/r)^{12} - (\sigma/r)^6] \tag{3}$$

$$v_{\alpha\gamma}^{coul}(r) = (z_\alpha z_\gamma e^2)/r \tag{4}$$

where $\mathbf{r}_i^\alpha$ denotes the coordinate of site α = O, H in the ith water molecule and e represents the electron charge.

TABLE 1: Parameters for Potentials

(a) SPC Model[a]

	σ (Å)	ϵ (kcal/mol)	charge (e)
O−O	3.17	0.156	
O			−0.82
H			0.41

(b) Solute−Solvent[b]

	z_i	B (10^3 kcal Å^{12}/mol)	C (kcal Å^6/mol)
Cl^-−O	−1	5765.8	2880.6
Cl^-−H	−1	13.3	138.2

[a] From ref 50. [b] From ref 51.

The interactions between the solute particles and water were also modeled using a standard (6-12) Lennard Jones term plus a Coulomb tail

$$V_{is} = \sum_{j,\alpha} u_\alpha^{is}(|\mathbf{r}_i - \mathbf{r}_j^\alpha|) \tag{5}$$

with

$$u_\alpha^{is}(r) = \frac{B_\alpha}{r^{12}} - \frac{C_\alpha}{r^6} + \frac{z_i z_\alpha e^2}{r} \tag{6}$$

In eqs 5 and 6, $\mathbf{r}_i$ and z_i identify the position and charge of the solute, respectively. To model the solute, we used the parameters corresponding to the Cl^- ion given by Pettit et al.;[51] neutral solutes, hereafter referred to as Cl, were modeled using the same Lennard-Jones parameters as for the chloride ion and setting $z_i = 0$. Full details of the parameters for the different potentials are presented in Table 1.

Two sets of simulation experiments were performed. The first one involved series of 300 ps molecular dynamics runs corresponding to the canonical ensemble[52] along the $T = 645$ K isotherm, which is 10% above the estimate of the critical temperature for the SPC model, $T_C^{SPC} \approx 587$ K.[53] The density interval extended from the standard liquid value for ambient conditions, i.e., $\rho = 1$ g cm^{-3}, down to $\rho = 0.3$ g cm^{-3}, which is also slightly above the computed critical density for the water model, $\rho_C^{SPC} \approx 0.27$ g cm^{-3}.[53] In choosing this temperature and density range, we deliberately tried to avoid any effects associated with criticality. The second kind of experiments corresponded to nonequilibrium trajectories: initial states were sampled from configurations generated by a canonical trajectory and separated by 5 ps intervals; this time was sufficiently long to yield statistically independent initial conditions. At $t = 0$, the Nosé thermostat[52] was removed, the charge of the solute was modified, and particle velocities were assigned according to the Boltzmann distribution; from these initial conditions, we followed the solvent relaxation for about 2 ps.

In all experiments the Verlet algorithm[54] was used to integrate the equations of motions using a time step of 1 fs; to handle intramolecular constraints in the solvent particles the SHAKE algorithm[55] was implemented. Since some the systems under investigation were not electrically neutral, we could not implement Ewald sums techniques[54] to handle long range Coulomb potentials; instead, all interactions were truncated at half of the simulation box length and brought smoothly to zero in an interval of 0.5 Å by a fourth-degree spline.

Nonequilibrium Experiments

We start our analysis by considering the temporal dependence of the dielectric response of supercritical water following the model ionization reaction

$$Cl \rightarrow Cl^- \tag{7}$$

For this particular process, the solvation dynamics can be conveniently described in terms of $S(t)$, the normalized nonequilibrium solvent response defined by

$$S(t) = \frac{\langle V_c(t) - V_c(\infty)\rangle_{ne}}{\langle V_c(0) - V_c(\infty)\rangle_{ne}} \tag{8}$$

where V_c represents the Coulombic contribution to the solute−solvent coupling at time t and $\langle ... \rangle_{ne}$ denotes an average sampled from a distribution of nonequilibrium initial conditions.[56]

Maroncelli et al.[34] have established the characteristics of $S(t)$ for water at 298 K. An important observation of their simulation study was that, despite the well-known structural features that make liquid water a peculiar fluid at ambient conditions, its dynamical response does not differ substantially from that of a typical aprotic polar solvent such as, for example, acetonitrile.[39] In both cases, the solvation responses present as a distinctive common feature a bimodal character, *i.e.*, an initial fast transient accounting for a major fraction of the total response and lasting a few hundreds of femtoseconds, followed by a much slower regime with characteristic time scale of the order of 1−5 ps.[57]

From a qualitative point of view, the characteristics of the dynamics of these two regimes are also well differentiated.[29,30] During the first inertial period, effects from translational movements can normally be neglected; solvent molecules carry out mostly fast librations or small amplitude rotations and move almost independently from one another with velocities dictated by the original Maxwell−Boltzmann distribution they had prior to the solute perturbation.[30] The second stage of the solvation is characterized by both rotational and translational diffusive motions that prevail for t larger than the time interval required for single-particle momentum correlations to decay; in most cases, this last portion of the response can be adequately reproduced assuming a single or biexponential decay.[34,39]

Figure 1 illustrates results for $S(t)$ corresponding to the process shown in eq 7 taking place at three different supercritical densities, ρ= 1, 0.65, and 0.3 g cm^{-3}; to establish a direct comparison with a similar process at ambient conditions, in Figure 2 results for $S(t)$ corresponding to $\rho = 1$ g cm^{-3} and $T = 298$ K are also displayed. The supercritical curves present two interesting features: (i) they maintain the bimodal character observed at room temperature, and (ii) the clear prominence of the inertial regime at the early stages of solvation gradually diminishes as we move toward lower densities. Consequently, the subsequent diffusive stage exhibits the opposite trend, accounting for a major portion of the total solvent relaxation at low densities and becoming almost negligible at $\rho = 1$ g cm^{-3} and $T = 645$ K.

A rough estimate of the time scale that characterizes the overall solvation process can be obtained from the average correlation time τ_s, defined as

$$\tau_s = \int_0^\infty S(t)\, dt \tag{9}$$

The data of the third column of Table 2 reveal that the solvent relaxation at $\rho = 1$ g cm^{-3} and $T = 645$ K lasts for about 50 fs, a time interval almost an order of magnitude smaller than those describing a similar process taking place at lower supercritical densities or at ambient conditions. To grasp the wide differences observed in these time scales, we tried to unveil microscopical details of the spatial and orientational correlations around the probe along the different stages of the relaxation.

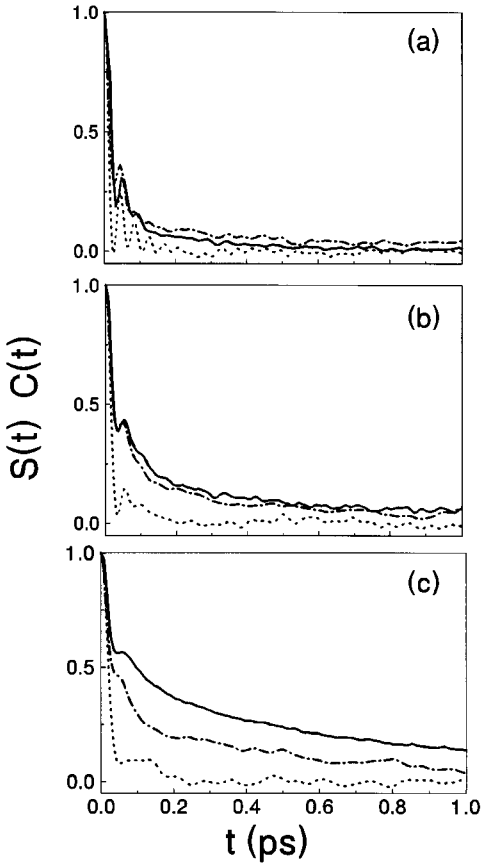

Figure 1. Dielectric response $S(t)$ (solid line) for supercritical SPC water at $T = 645$ K at different densities. (Top panel) $\rho = 1$ g cm^{-3}; (middle panel) $\rho = 0.65$ g cm^{-3}; (lower panel) $\rho = 0.3$ g cm^{-3}. Also shown the corresponding equilibrium time correlation functions $C(t)$ for charged (dashed−dotted line) and neutral (dotted line) solutes.

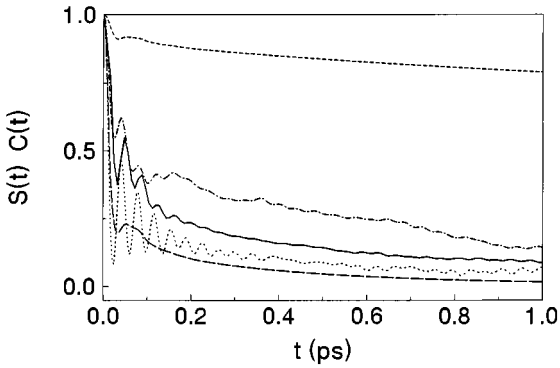

Figure 2. Same as Figure 1 for SPC water at ambient conditions. Also shown are the single dipole−dipole autocorrelation function (short dashed line) and predictions for $C(t)$ computed from eq 17 (long dashed line).

We started by considering some general aspects of the equilibrium solute−solvent spatial correlations for charged and neutral solutes dissolved in supercritical water. Figure 3 contains results for $g_{Cl-\gamma}$ (γ = O, H), the solute−oxygen and solute−hydrogen radial distribution functions for the highest and lowest densities considered in this study. The simultaneous analysis of these plots and the entries of Table 3 may be helpful to interpret the main characteristics of the different equilibrium solvation structures. At $\rho = 1$ g cm^{-3} and $T = 645$ K, the equilibrium solute−solvent spatial correlations for a neutral solute does not differ substantially from those computed for a rare gaslike particle of similar size, say a Kr atom, dissolved in water at room temperature.[58] In particular, $g_{Cl-O}(r)$ presents a

TABLE 2: Solvation Parameters for Water

ρ (g cm^{-3})	T (K)	τ_s^a (ps)	ω_s^b (ps^{-1})	ω_1^c (ps^{-1})	$(\omega_s/\omega_1)^2$	α_s^d	10^{-2} f_s	ω_s^{INM} (ps^{-1})
0.3	645.15	0.57	55.8	≃34	2.7	3.06	1.8	54.3
0.65	645.15	0.21	76.8	≃34	5.1	5.4	1.5	71.4
1.0	645.15	0.05	100.0	≃34	8.7	8.0	1.1	92.4
1.0	298.15	0.41	104.8	≃23	20.8	17.4	1.4	111.4

[a] Calculated from the experimental $S(t)$ up to 1.5 ps; after that time a single-exponential decay was assumed. [b] Computed from the best Gaussian fit of $C(t)$ over the interval $t < 50$ fs. [c] From ref 44. [d] Computed from eq 16 and estimated bulk dielectric constants from refs 15a and 17.

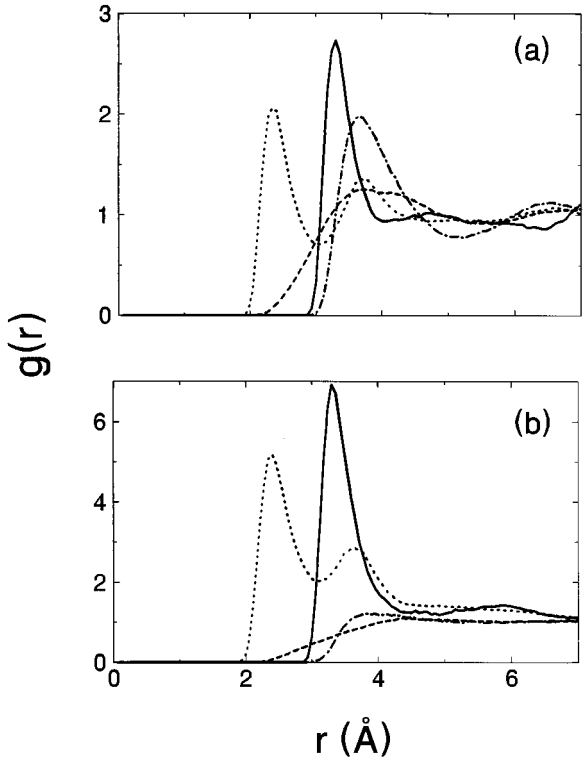

Figure 3. Equilibrium solute−solvent radial distribution functions for supercritical water at different densities. (Top panel) $\rho = 1$ g cm^{-3}; (bottom panel) $\rho = 0.3$ g cm^{-3}. g_{Cl-O} (dashed−dotted line); g_{Cl-H} (dashed line); g_{Cl^--O} (solid line); g_{Cl^--H} (dotted line).

first solvation shell located at $r_{max} = 3.66$ Å containing roughly $N \approx 16-17$ solvent molecules and extending up to $r_{min} = 5.22$ Å; the presence of a single broad maximum in $g_{Cl-H}(r)$ located at a similar distance would suggest that the hydrogen atoms lie at straddled configurations such that the orientation of the individual water dipoles remain mostly perpendicular to the radial Cl−O axis. The solute−oxygen pair distribution distributions for the ionic solute presents a much higher and narrower first peak slightly shifted toward smaller distances that contains $N \approx 8$ eight solvent molecules. The profile corresponding to $g_{Cl^--H}(r)$ also exhibits important changes; most notably, the splitting of the first peak. In this respect, we note two important features: a first sharp maximum at 2.34 Å containing 6.3 atoms that represents the fingerprint of the hydrogen-bonding characterizing solute−solvent interactions and the position of the second peak at 3.72 Å, indicative of the linear arrangement of the Cl$^-$−H−O group.

Results of the lower panel of Figure 3 correspond to $\rho = 0.3$ g cm^{-3}. The contrast between the originally quite blurred structures of g_{Cl-O} and g_{Cl-H}—both characterized by broad and flat profiles that hardly exceed unity—and the highly structured first solvation shell for the ionic solute is self-evident. The considerable magnitude of $g_{Cl^--O}(r_{max}) \approx 6.9$ puts in evidence a significant enhancement of the local solvent density around the ion compared to the average bulk value; this solvent aggregation occurs as a consequence of the high compressibility

TABLE 3: Selected Characteristics of the Solute−Solvent Radial Distribution Functions for Neutral and Charged Solutes

(a) g_{Cl-O}

ρ (g cm^{-3})	r_{max} (Å)	g_{Cl-O} (r_{max})	r_{min} (Å)	N	N_1
0.3	3.85	1.21	5.28	5.0	4.2
0.65	3.84	1.36	5.76	14.0	8.9
1.0	3.66	1.98	5.22	16.6	16.6

(b) g_{Cl^--O}

ρ (g cm^{-3})	r_{max} (Å)	g_{Cl^--O} (r_{max})	r_{min} (Å)	N	N_1
0.3	3.30	6.92	4.92	9.0	9.5
0.65	3.36	3.82	4.32	8.0	11.3
1.0	3.30	2.73	4.08	7.9	15.4

(c) g_{Cl-H}

ρ (g cm^{-3})	r_{max} (Å)	g_{Cl-H} (r_{max})	N
0.3	4.40	1.10	*a*
0.65	4.50	1.14	*a*
1.0	3.72	1.25	38.6

(d) g_{Cl^--H}

ρ (g cm^{-3})	r_{max} (Å)	g_{Cl^--H} (r_{max})	N
0.3	2.40	5.18	5.6
0.65	2.40	2.91	6.5
1.0	2.34	2.06	6.3

[a] Simulation results are too noisy to clearly determine a first solvation shell.

of the environment that allows large fluctuations in the local density around strongly interactive solutes.[8,14,59] Note, however, that the position of the first solvation shell, $r_{max} = 3.3$ Å, and the number of solvent nearest neighbors, $N = 9$, are comparable to those obtained for $\rho = 1$ g cm^{-3}. The absence of significant changes would suggest that even in supercritical systems exhibiting bulk densities close to what one would consider as typical for a highly dense vapor environment, electrostatic interactions are sufficiently strong to bring the first solvation shell to a near saturation maintaining similar characteristics of the solute−solvent hydrogen bonding to those observed in much denser fluids.

Having established the characteristics of the limiting distributions, we now turn to the dynamical analysis of solvation. In Figure 4 we present results for the relaxations of the solute−oxygen radial distribution functions at selected time intervals following the initial charge jump. The transients of g_{Cl^--O} corresponding to $\rho = 1$ g cm^{-3} show that the total rearrangement of the solvation structure requires approximately 200 fs since the nonequilibrium radial distribution computed at that time is virtually identical with the limiting $t \rightarrow \infty$ equilibrium result for an ionic solute. These results should be contrasted to those shown in the bottom panel of Figure 4 that correspond to $\rho = 0.3$ g cm^{-3}; note that g_{Cl^--O} computed at $t = 800$ fs still differs considerably from the final equilibrium, i.e., $t \rightarrow \infty$, profile. Although the previous observations corroborate the density trends already found for τ_s, we still lack a clear physical interpretation of the dynamical mechanisms through which the different relaxations take place. To gain some additional insight,

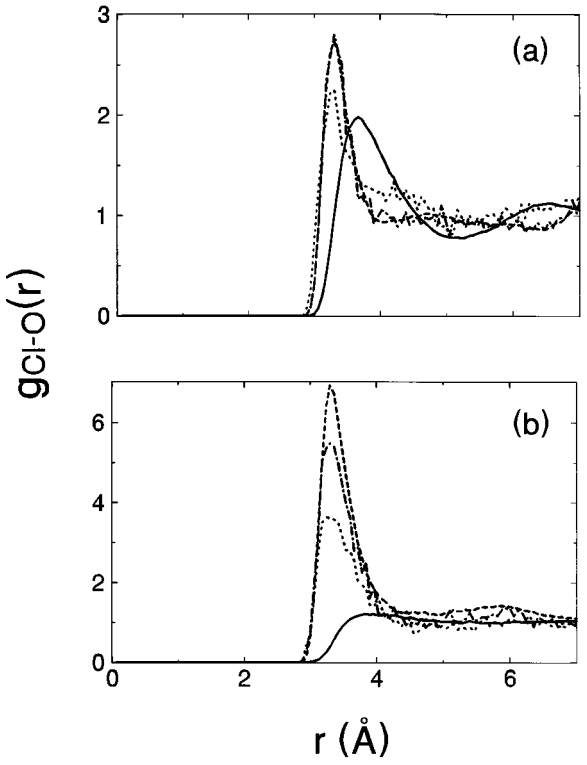

Figure 4. Transients of $g_{Cl^-–O}$ in supercritical water at different densities. (a) $\rho = 1$ g cm^{-3}; $t = 0$ fs (solid line), $t = 100$ fs (dotted line), $t = 200$ fs (dashed−dotted line), $t = \infty$ (dashed line). (b) $\rho = 0.3$ g cm^{-3}; $t = 0$ fs (solid line), $t = 500$ fs (dotted line), $t = 800$ fs (dashed−dotted line), $t = \infty$ (dashed line).

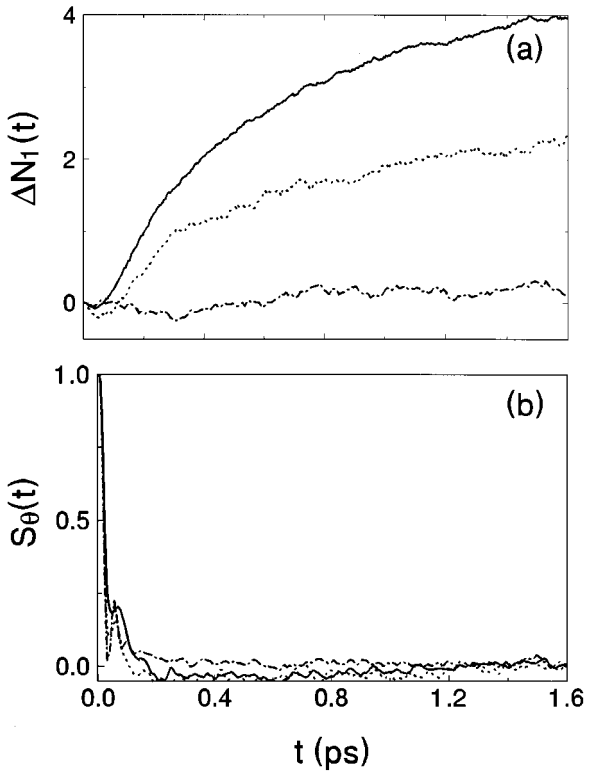

Figure 5. Nonequilibrium solvent population $\Delta N_1(t)$ (top panel) and angular relaxation, $S_\theta(t)$, (bottom panel) for supercritical water at different densities (see text). $\rho = 1$ g cm^{-3} (dashed−dotted lines); $\rho = 0.65$ g cm^{-3} (dotted lines); $\rho = 0.3$ g cm^{-3} (solid lines).

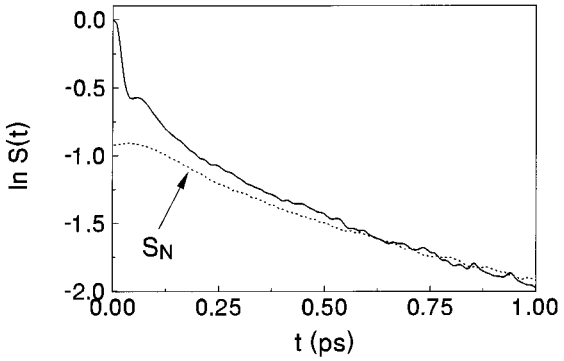

Figure 6. Nonequilibrium solvation response for supercritical water at $T = 645$ K and $\rho = 0.3$ g cm^{-3}. Also shown is the normalized population relaxation $S_N(t)$ (see text) shifted in the vertical axis by −0.92.

we also monitored the relaxation of $N_1(t)$, the solvent population within a fixed volume whose boundary was arbitrarily chosen at the position of the first minimum $r_{min} = 5.22$ Å of $g_{Cl–O}$ at $\rho = 1$ g cm^{-3}. Figure 5a contains results for $\Delta N_1(t) = N_1(t) - N_1(0)$ computed for three different densities. In all cases, the sudden switch of solute−solvent Coulomb forces produces a small, although perfectly noticeable, reduction in $\Delta N_1(t)$ during a time interval that is very brief for the two lowest solvent densities—lasting a few tens of a femtosecond—and somewhat longer for $\rho = 1$ g cm^{-3} where the highly packed structure of the fluid leads to a rearrengement of the solvent particles around the solute somewhat slower. Anyhow, on the basis of the virtual constancy of $N_1(t)$ for the high-density case at all subsequent times, one could reasonably discard any relevant contribution to $S(t)$ arising from translational movements during, say, the first 150 fs, the time interval during which 90−95% of the total relaxation of $S(t)$ takes place. The long time behavior of $\Delta N_1(t)$ at lower densities is completely different and presents a slower relaxation branch with characteristic times on the order of a few picoseconds. This portion of the relaxation is clearly indicative of the gradual approach of the solvent molecules originally located far away from the solute and provides a clue about the nature of the dynamics associated with the long-time decay of $S(t)$. A conclusive test is presented in Figure 6; the similarities between the long time logarithmic decays of $S(t)$ and $S_N(t)$ defined by

$$S_N(t) = \frac{\langle N_1(t) - N_1(\infty)\rangle_{ne}}{\langle N_1(0) - N_1(\infty)\rangle_{ne}} \tag{10}$$

for $\rho = 0.3$ g cm^{-3} confirm the diffusive character of the second half of the solvation response. We finally considered some aspects of the rotational response of the solvent by computing $S_\theta(t)$, the normalized nonequilibrium correlation function for $\cos[\theta(t)]$ defined as

$$\cos(\theta) = \frac{1}{N_1}\sum_{j=1}^{N_1}\frac{(\mathbf{r}_i - \mathbf{r}_j^\circ)\cdot\mu_j}{|\mathbf{r}_i - \mathbf{r}_j^\circ|\cdot|\mu_j|} \tag{11}$$

where μ_j represents the dipole moment of the jth water molecule. The results are shown in Figure 5b. In all cases—including the results for ambient conditions also shown in the figure—the relaxations of $\cos[\theta(t)]$ present an extremely fast decay that accounts for about 90% of the total response followed by few small amplitude, underdamped oscillations that are more evident at higher densities. Although the curves of Figure 5b present practically identical characteristics, we tend to believe that the mechanisms that drive the rotational responses should not be the same in all cases. At low densities, the solvent intercoupling is rather weak and one could in principle ascribe a major portion

of the fast orientational decay to free, almost independent, individual rotations of the solvent molecules. On the other hand, as the density of the solvent gets higher, the mechanisms for the orientational relaxation of the solvent would involve mostly collective, small amplitude, librational motions. Since the three moments of inertia of the water molecule are rather small, the solvent has many open channels available for rotational relaxation. Consequently, a major portion of the rotational response can be achieved in a brief interval and at a relatively low energy cost since it inflicts minor disruptions in the original solvent−solvent structure. We will return to more important considerations of collective vs individual rotational mechanisms for relaxation when we consider the behavior of equilibrium time correlation functions that, for clarity purposes, we prefer to postpone to the following sections.

4. Linear Response Predictions

The fluctuation−dissipation theorem[56] provides an alternative route through which it is possible to estimate nonequilibrium relaxations via equilibrium time correlation functions, provided the hypothesis of linear response theory are satisfied. For sufficiently small perturbations, the nonequilibrium response $S(t)$ can be approximated by

$$S(t) \simeq C(t) = \frac{\langle \delta V_c(t)\, \delta V_c(0) \rangle}{\langle (\delta V_c)^2 \rangle} \tag{12}$$

where $\langle ... \rangle$ denotes an equilibrium ensemble average and $\delta V_c(t) = V_c(t) - \langle V_c \rangle$ represents spontaneous fluctuations of the solvent electrical potential upon the solute. Previous simulations of aqueous solutions at room temperature[34,35,42,43] have shown that predictions from linear response theory describe remarkably well the time behavior of $S(t)$ even for those cases where the energy difference between the initial and final solute−solvent coupling is well beyond the range of accessible thermal energies.

The performance of linear response theories for aqueous solvation at supercritical conditions is indicated in Figure 1, where we have included results of $C(t)$ for neutral and charged solutes. At $\rho = 1$ g cm^{-3}, both equilibrium time correlation functions provide reasonable estimates for the nonequilibrium curve during the whole relaxation process; the quality of the agreement between the computed $C(t)$ and $S(t)$ is similar to that found at room temperature (cf. Figure 2) where $S(t)$ lies between both equilibrium correlation functions. Furthermore, note that the supercritical curve still maintains a short transient characterized by fast underdamped oscillations with a period of about 20−25 fs bridging the inertial and diffusional regimes. These oscillations, which represent a distinctive feature of the equilibrium correlation function of water at room temperature, have been interpreted as hydrogen bond librations.[31,34,60] As we move toward lower densities, the results from Figure 1b,c reveal that predictions from linear response theory become progressively less accurate. While at $\rho = 0.65$ g cm^{-3}, the agreement between the equilibrium and nonequilibrium responses could still be considered acceptable, it is evident that both equilibrium time correlation functions computed at $\rho = 0.3$ g cm^{-3} present a much faster decay than the actual dielectric response.

Why does this breakdown happen? In principle, one could argue that the applied charge perturbations are sufficiently strong so that the main hypothesis supporting linear theories is not fully satisfied. But if this is so, one could still wonder why the theory works reasonably well when a similar perturbation is applied at higher densities. To account for this behavior, we can bring into consideration the following explanation: as noted by Fonseca et al.,[37] linear response theories are expected to be adequate provided the initial inertial response—which is the portion that depends on the equilibrium distribution prior to the charge jump and remains virtually unaffected by the actual size of the perturbation—represents the predominant contribution to the total response. This is clearly the situation at high densities where the inertial regime constitutes almost 80% of the total response; however, note that this contribution diminishes to approximately 60% at $\rho = 0.65$ g cm^{-3} and 40% at $\rho = 0.3$ g cm^{-3}. In addition, the extent of the contribution of the initial inertial response also depends on the characteristics of the solute−solvent coupling; linear response theory predictions for the solvation response of aqueous systems are much more accurate for ionic solutes than for dipolar ones.[49] Second, one should not expect that equilibrium time correlation functions could predict even approximately the important contributions to the slower diffusional portion of the nonequilibrium response arising from gradual clustering of the solvent particles around the newly created ionic solute. This would require spontaneous fluctuations of the local solvent density around neutral solutes similar in size to those found for charged probes, which of course, are highly unlikely. Consequently, it is not surprising that in this density range both equilibrium correlation functions present a much faster decay than $S(t)$ and that predictions from linear response theory remain valid during shorter time intervals.

We will now address another important aspect connected to the earliest stages of solvation, the period during which the decays of $C(t)$ and $S(t)$ are still comparable. We have already mentioned that during the first 50−100 fs following the initial perturbation of the solute, the overall dynamics of the solvent can be described as a free streaming of the individual molecules. Several simulation experiments have confirmed that during that period $C(t)$ can be reasonably well approximated by a simple Gaussian function of the form[29,30]

$$C(t) \simeq \mathrm{e}^{-(1/2)\omega_s^2 t^2} \tag{13}$$

In the last equation we have introduced the solvation frequency ω_s, an equilibrium quantity that determines the width and the initial curvature of the response. Using simple physical arguments, Maroncelli et al.[44] have derived the following relation between ω_s^2 and ω_1^2, the average squared free rotational frequency of a water molecule, namely

$$\omega_s^2 \simeq \alpha_s \omega_1^2 \tag{14}$$

where

$$\omega_1^2 = \frac{2k_B T}{I_{eff}} \tag{15}$$

In the last equation, k_B is the Boltzmann constant and I_{eff} is a weighted sum of moments of inertia along different principal axes of the solvent molecule.[61] Assuming the Born model for solvation, Maroncelli et al. found that the factor α_s can be expressed in terms of parameters of the solvent as follows

$$\alpha_s = \frac{4\pi\rho\mu^2}{3k_B T}\left(1 - \frac{1}{\epsilon}\right)^{-1} \tag{16}$$

where ϵ represents the bulk dielectric constant of the medium. In the sixth column of Table 2 we present ratios of $(\omega_s/\omega_1)^2$ obtained from the best Gaussian fit of the neutral $C(t)$ during the initial 50 fs; in column seven results for α_s calculated from eq 16 are also displayed. In light of the simplicity of the hypothesis that leads to eq 14 and the wide intervals of temperature, density, and solvent polarization considered in this

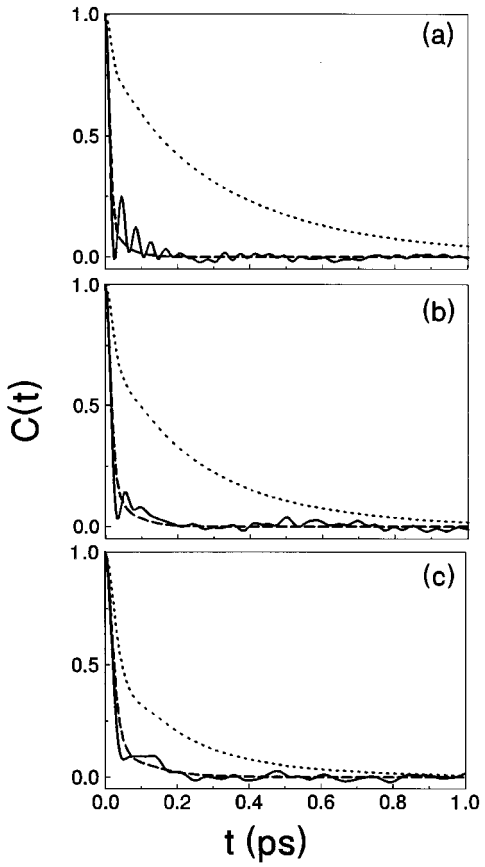

Figure 7. Equilibrium time correlation functions $C(t)$ for an uncharged solute at different supercritical states. (a) $\rho = 1$ g cm^{-3}; (b) $\rho = 0.65$ g cm^{-3}; (c) $\rho = 0.3$ g cm^{-3}. Simulation results (solid lines); predictions from eq 17 (dashed lines). Also shown are the individual dipole−dipole correlation functions for the neat liquid (dotted line).

study (including the room-temperature case), the quality of agreement between the two sets of results is quite remarkable. If the solvation mechanism presents a dipolar character, one can even move one step forward and establish a connection between the individual dipolar correlation and the equilibrium time correlation function. For polar solvents, $C(t)$ can be normally well represented at all times by[44]

$$C(t) \simeq \langle \hat{u}(t)\cdot\hat{u}(0)\rangle^{\alpha_s} \tag{17}$$

where $\langle \hat{u}(t)\cdot\hat{u}(0)\rangle$ is the autocorrelation function for single dipolar orientation for the pure solvent. The power α_s in the previous expression should now be interpreted as a measure of up to what extent the solvent is able to relax a significant portion of its response via individual rotations; for a polar and highly structured liquid such as liquid water at 298 K, these motions normally promote a much slower decay of $\langle \hat{u}(t)\cdot\hat{u}(0)\rangle$. In Figure 7 we present results for the predictions of $C(t)$ based on the expression given in eq 17. We first remark the disparities in the temporal decays of $\langle \hat{u}(t)\cdot\hat{u}(0)\rangle$ between the supercritical states and the room-temperature case also shown in Figure 2. The faster decays of the former curves reveal the gradual loss of the orientational correlation that characterizes water at ambient conditions. However, despite the evident differences in the individual orientational correlations shown in the figures, predictions from eq 17 are in excellent agreement in all cases with the computed $C(t)$, confirming that the solvation mechanisms at supercritical conditions still can be reasonably well interpreted on the basis of an individual orientational motion description.

5. Dynamics of Solvation and Instantaneous Normal Modes

5.1. Brief Overview of the Formalism. Recently, Stratt and collaborators[62] have developed an alternative approach to investigate the dynamics of the early stages of solvation based on the examination of the instantaneous normal modes (INM) of the solvent. Since the solvation in polar solvents represents a complex process involving a high degree of cooperativity between a manifold of solvent degrees of freedom, the idea of conceiving these collective movements as sum of individual contributions from a set of uncoupled harmonic modes may facilitate considerably the interpretation of the characteristics of the solvation dynamics. For clarity purposes, we will present here a brief description of the main results of the formalism and we refer the reader interested in a more detailed presentation to refs 62−69.

The idea is conceptually simple: consider the system of N_w water molecules of total mass M described by a set of coordinates $\{\mathbf{R}_N\}$, $\mathbf{R}_i = X_i, Y_i, Z_i, \theta_i, \phi_i$, and ψ_i, where, as usual, X_i, Y_i, and Z_i represent the Cartesian coordinates of the center of mass of the ith molecule and θ_i, ϕ_i, and ψ_i, the Euler angles measured from a fixed laboratory frame. Imagine now performing a Taylor expansion of the total potential energy of the system at a given time t, $V[\mathbf{R}_N(t)]$, around an initial value of the potential evaluated at $t = 0$, $V[\mathbf{R}_N(0)]$. Keeping up to quadratic terms, the short time dynamics of the $6N_w$ coordinates can be recasted in a much simpler form by considering a set of generalized coordinates $q_\alpha(t; \mathbf{R}_N(t))$, $\alpha = 1, ..., 6N_w$, each one representing a collective mode whose dynamics corresponds to that of a harmonic oscillator of frequency ω_α. The set of INM frequencies $\{\omega_\alpha\}$ can be obtained in the usual way, i.e., by diagonalizing the $6N_w \times 6N_w$ generalized Hessian matrix $\mathbf{U}$ defined as

$$U_{i\mu,j\nu} = \frac{\partial^2 V}{\partial r_{i\mu}\partial r_{j\nu}} \tag{18}$$

To establish the natural distinction between translational and rotational modes, in the previous equation it was convenient to introduce $\{\mathbf{r}_{i\mu}\}$, $1 \le i \le N_w$ and $\mu = 1, 2, ..., 6$, a set of $6N_w$-dimensional mass-weighted center of mass and orientation generalized coordinates given by

$$\mathbf{r}_{i\mu} = \{\sqrt{M}X_i, \sqrt{M}Y_i, \sqrt{M}Z_i, \sqrt{I_x}\xi_{ix}, \sqrt{I_y}\xi_{iy}, \sqrt{I_z}\xi_{iz}\} \tag{19}$$

that should not be mistaken with a site coordinate; I_x represents the moment of inertia along the principal molecular axis x. The expression for the set of orientational degrees of freedom $\{\xi_{ix}\}$ can be obtained as follows

$$\begin{pmatrix}\xi_{ix}\\ \xi_{iy}\\ \xi_{iz}\end{pmatrix} = \begin{pmatrix}\cos\psi_i^0 & \sin\theta_i^0\sin\psi_i^0 & 0\\ -\sin\psi_i^0 & \sin\theta_i^0\cos\psi_i^0 & 0\\ 0 & \cos\theta_i^0 & 1\end{pmatrix}\begin{pmatrix}\theta_i\\ \phi_i\\ \psi_i\end{pmatrix} \tag{20}$$

where θ_i^0 and ψ_i^0 are the Euler angles evaluated at the instantaneous configuration $\{\mathbf{r}_{i\mu}(0)\}$ and are considered as constants.

5.2. Frequency Spectra of Supercritical Water. Before considering the INM analysis of aqueous solvation, it will be useful to briefly comment on the main features of the frequency spectra[66] of the supercritical neat liquid, $D(\omega)$, defined as

$$D(\omega) = \left\langle \frac{1}{6N_w}\sum_{\alpha=1}^{6N_w}\delta(\omega - \omega_\alpha)\right\rangle \tag{21}$$

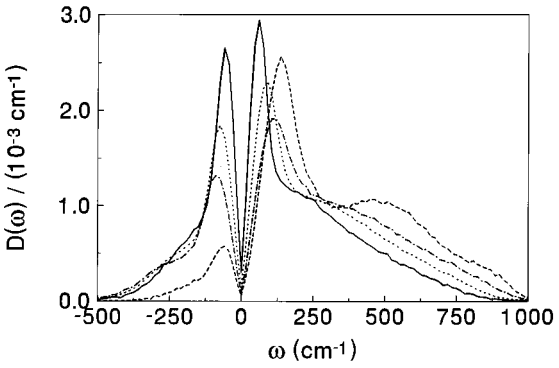

Figure 8. Instantaneous normal-mode frequency spectra for supercritical SPC water at $T = 645$ K: $\rho = 1$ g cm^{-3} (dashed−dotted line), $\rho = 0.6$ g cm^{-3} (dotted line), and $\rho = 0.3$ g cm^{-3} (solid line). Also shown is the spectrum for SPC water at ambient conditions (dashed line). In all cases, contributions from the zero-frequency modes have been subtracted.

For molecular systems, one can decompose the frequency spectrum into contributions from collective movements with well-differentiated characteristics. The generalized set of coordinates described in eq 19 is particularly suitable to construct translational and rotational projectors expressed in terms of the eigenvector matrix **W** as[64]

$$P_\alpha^{\mathrm{T}} = \sum_{j=1}^{N_w}\sum_{\mu=1}^{3}(W_{\alpha,j\mu})^2 \tag{22}$$

$$P_\alpha^{\mathrm{R}} = \sum_{j=1}^{N_w}\sum_{\mu=4}^{6}(W_{\alpha,j\mu})^2$$

where

$$(\mathbf{WUW}^{\mathrm{Tr}})_{\alpha\alpha'} = \omega_\alpha^2\delta_{\alpha\alpha'} \tag{23}$$

From these projectors, the corresponding translational and rotational contributions to the total frequency spectra are given by

$$D^{\mathrm{T}}(\omega) = \left\langle \frac{1}{6N_w}\sum_{\alpha=1}^{6N_w} P_\alpha^{\mathrm{T}}\,\delta(\omega-\omega_\alpha)\right\rangle \tag{24}$$

$$D^{\mathrm{R}}(\omega) = \left\langle \frac{1}{6N_w}\sum_{\alpha=1}^{6N_w} P_\alpha^{\mathrm{R}}\,\delta(\omega-\omega_\alpha)\right\rangle$$

with $D(\omega) = D^{\mathrm{T}}(\omega) + D^{\mathrm{R}}(\omega)$.

In Figures 8 and 9 we present plots of $D(\omega)$, $D^{\mathrm{T}}(\omega)$, and $D^{\mathrm{R}}(\omega)$ for different supercritical states. The results were obtained by averaging over 100 solvent configurations taken from a canonical trajectory and separated by 2 ps intervals; as it is customary, the negative frequency portions of the spectra correspond to imaginary frequencies. The characteristics of the translational and rotational contributions to the total density of modes at supercritical conditions are similar to those found at room temperature: translational modes prevail at low frequencies, say for $\omega \leq 250$ cm^{-1}, and in the imaginary portion of the spectra, while rotational modes become predominant at high frequencies. A closer inspection, however, reveals that the change in temperature at constant density provokes in the positive branch a reduction of the translational and rotational spectra with minor changes in the shapes and positions of the respective maxima; of course, since all spectra are normalized

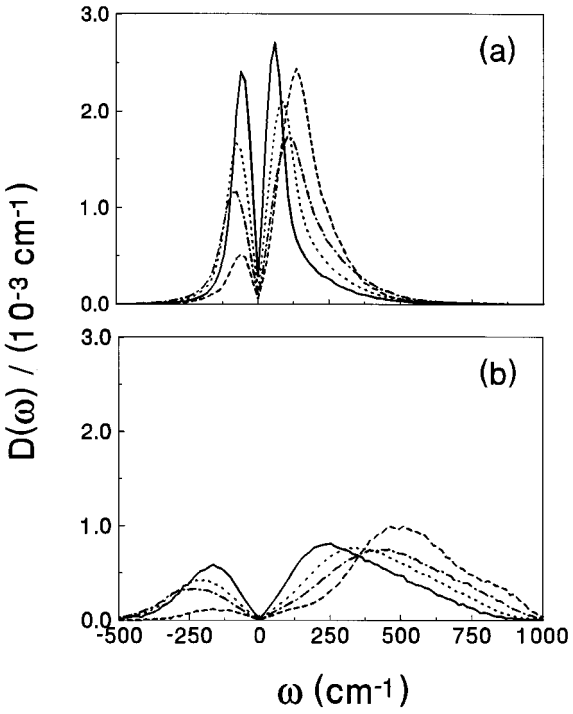

Figure 9. Translational (top panel) and rotational (bottom panel) contributions to the instantaneous normal-mode frequency spectra for supercritical SPC water at $T = 645$ K at different densities. Same labeling as Figure 8.

to unity, these changes are compensated with opposite trends in the unstable frequency portions. On the other hand, a density reduction at constant temperature causes shrinkages from both wings: in the real-frequency part, the contributions from high-frequency rotational modes become progressively less important and the main translational peak increases considerably as it shifts toward smaller frequencies; concomitantly, the imaginary frequency lobe of the spectra also gets somewhat narrower and much higher. The fraction of imaginary modes presents a moderate growth from 0.22 for $\rho = 1$ g cm^{-3} up to 0.33 for $\rho = 0.3$ g cm^{-3}.

The dynamical model proposed by Zwanzig[70] can be of some help to rationalize part of these changes. Zwanzig's picture considers the fluid as a collection of cells where the molecules perform nearly harmonic oscillations around different local minima.[71] Diffusion takes place due to jumps over saddle points that destroy the coherence of the harmonic dynamics; the jump frequency, ω_v, determines the corresponding hopping rate that may present an Arrhenius-like dependence with temperature.[72] It is obvious that a reduction in the fluid density leads to larger interparticle distances and to less pronounced curvatures of the potential energy surface. As the heights of the barriers that separate the manifold of potential wells decrease, thermal fluctuations can promote more frequent jumps between local trapping sites and configurations in which the molecules lie in regions of negative curvature are more likely to occur. Consequently, the connection between the fraction of unstable modes and diffusion comes as a rather intuitive result. However in the present context, this line of reasoning has one important restriction namely, even if we are willing to accept this activated mechanism for the diffusion, the applicability of the model should be less justifiable as we move toward vaporlike environments. In other words, it is evident that the harmonic dynamics should remain valid for $t \ll \omega_v^{-1}$; although there are ways to estimate ω_v^{-1}, it will be sufficient to say at this point that this characteristic time should decrease considerably as we move

toward lower densities. Thus, the problem still is whether the process whose dynamics we are interested in describing lasts less than the characteristic time that describes the changes in the instantaneous curvature of the potential energy surface. As we have seen in previous sections, the major portion of the solvation response of supercritical water comes from an extremely fast early stage, so one can reasonably guess that the INM formalism will still provide meaningful results for the solvation response.

Although the supercritical spectra of Figures 8 and 9 present clear trends in their density dependences, it is also evident that the overall low-density structures resemble to a considerable extent results corresponding to $\rho = 1$ g cm^{-3} or even those computed at room temperature. Given the obvious differences of the microscopic structures of a highly packed liquid and a dense steam, the persistence of such a degree of similarity in the topography of the potential energy surface is rather surprising. To make this point even more clear, the comparison with the supercritical INM spectra of a less structured fluid can be instructive. For example, consider the recent study of Kalbfleich et al.[73] dealing with the solvation response of supercritical argon following an electronic transition of an infinite diluted CH_3I probe at 298 K. If we disregard the differences in the reduced temperatures that prevent a direct correspondence between both sets of results, the INM spectra of supercritical argon show dramatic changes with density: while the spectrum for a typical liquid density, $\rho\sigma^3 = 0.8$, presents a broad real-frequency portion spanning up to approximately 100−150 cm^{-1}, the one corresponding to $\rho\sigma^3 \simeq 0.3$—which measured in terms of the packing fraction is similar to the lowest density state presented in this study—collapses into two sharp peaks flanking the zero-frequency region with almost no structure beyond 10 cm^{-1}.[73] On the basis of the previous observation, it would seem that supercritical water retains the "essence" of the structure of its room-temperature potential energy surface quite intact.

The analysis of the participation ratios[66] would lead to similar conclusions. In particular, we have computed

$$R_\alpha^{\mathrm{I}} = \sum_{j\mu} (W_{\alpha,j\mu})^4 \tag{25}$$

$$R_\alpha^{\mathrm{II}} = \sum_j [\sum_\mu (W_{\alpha,j\mu})^2]^2 \tag{26}$$

the reciprocals of R_α^{I} and R_α^{II} are indicative of the number of degress of freedom and the number of molecules contributing to the αth mode, respectively. Results for the participation ratios for the stable mode portion of the spectra are shown in Figure 10; attention should be paid to the fact that the curves, although normalized by the corresponding densities of states, still depend on the size of the simulated system. The results for $\rho = 1$ g cm^{-3} and $T = 645$ K show a considerable degree of collectiveness in the majority of the harmonic displacements with the exception of the high-frequency wing. To provide a rough quantitative idea of the extent of delocalization in the dynamics, we estimated the fraction of modes that involve less than one-quarter of the total number of molecules as reflected by the region of the spectrum where $(R^{\mathrm{II}})^{-1}$ falls below $30 \simeq N_w/4$. At $\rho = 1$ g cm^{-3}, that region is characterized by $\omega > 690$ cm^{-1} and encompasses only 4% of the modes; these results are quite close to those of room temperature where we obtained a slightly smaller percentage, 2%, and the threshold frequency shifted to $\omega = 840$ cm^{-1}. The gradual loss of correlation in the harmonic displacements of different particles in vaporlike environments is clearly reflected by the localization of the modes in fewer degrees of freedom; for $\rho = 0.3$ g cm^{-3}, the percentage of modes involving less than 30 molecules attains 25%. We finally note the complete disappearance of the dip that exists in the intermediate frequency region of the room-temperature spectra, also observed in the quenched normal mode spectrum.[66]

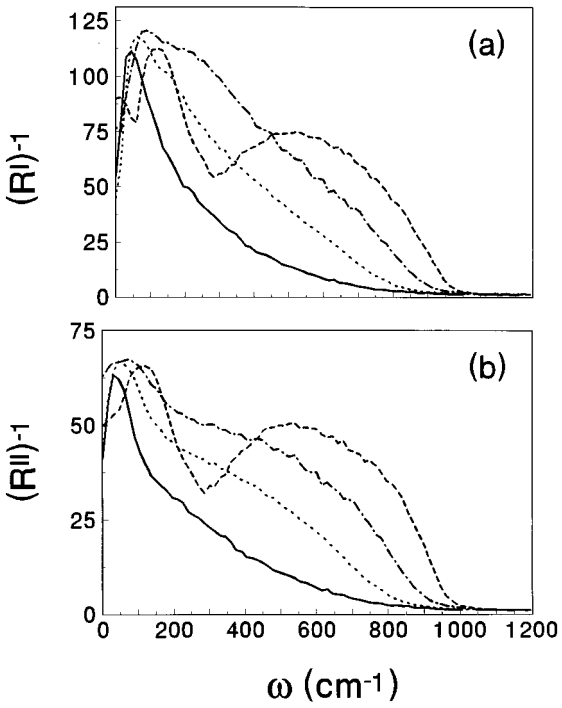

Figure 10. Inverse participation ratios for supercritical water. Only the stable modes are shown. $(R^{\mathrm{I}})^{-1}$ (top panel) and $(R^{\mathrm{II}})^{-1}$ (bottom panel). Same labeling as Figure 8.

5.3. Solvation Spectra of Supercritical Water. The INM approach can be extended in a natural way to compute the short time evolution and the corresponding correlation functions for any physical observable that can be expressed as an analytical function of the coordinates. To establish contact with our previous results, we focus attention on $C(t)$ for the uncharged solute. Following Stratt and Cho,[65] we expand V_c up to linear order in the set $\{q_\alpha\}$

$$V_c(t) = V_c(0) + \sum_\alpha \frac{\partial V_c}{\partial q_\alpha} q_\alpha(t) \tag{27}$$

After a few manipulations, the equilibrium time correlation function $C(t)$ can be expressed as

$$C(t) = 1 - \frac{k_B T}{\langle(\delta V_c)^2\rangle_{z_i=0}} \int D_s(\omega) \frac{1 - \cos(\omega t)}{\omega^2} \mathrm{d}\omega \tag{28}$$

where we have introduced the solvation spectrum $D_s(\omega)$ defined by

$$D_s(\omega) = \left\langle \sum_\alpha \left(\frac{\partial V_c}{\partial q_\alpha}\right)^2 \delta(\omega - \omega_\alpha) \right\rangle_{z_i=0} \tag{29}$$

and $\langle ... \rangle_{z_i=0}$ represents an average computed with a neutral solute. Operating in a similar way as we did for the total spectrum case, it is also possible to decompose $D_s(\omega)$ into translational, rotational, and cross contributions, namely[64,65]

$$D_s(\omega) = D_s^{\mathrm{T}}(\omega) + D_s^{\mathrm{R}}(\omega) + D_s^{\mathrm{C}}(\omega) \tag{30}$$

where

$$D_s^T(\omega) = \langle \sum_{\alpha=1}^{6N_w} (S_\alpha^T)^2 \delta(\omega - \omega_\alpha) \rangle_{z_i=0} \quad (31)$$

$$D_s^R(\omega) = \langle \sum_{\alpha=1}^{6N_w} (S_\alpha^R)^2 \delta(\omega - \omega_\alpha) \rangle_{z_i=0} \quad (32)$$

$$D_s^C(\omega) = \langle \sum_{\alpha=1}^{6N_w} S_\alpha^T S_\alpha^R \delta(\omega - \omega_\alpha) \rangle_{z_i=0} \quad (33)$$

and

$$S_\alpha^T = \sum_j \sum_{\mu=1,3} \frac{\partial V_c}{\partial r_{j\mu}} \frac{\partial r_{j\mu}}{\partial q_\alpha} \quad (34)$$

$$S_\alpha^R = \sum_j \sum_{\mu=4,6} \frac{\partial V_c}{\partial r_{j\mu}} \frac{\partial r_{j\mu}}{\partial q_\alpha} \quad (35)$$

Plots of the solvation spectra for two densities are shown in Figure 11. As a first striking feature, we note that the differences between $D_s(\omega)$ and $D_s^R(\omega)$ are practically imperceptible within the scale of the figures, revealing that the overwhelming majority of the solvation modes presents a well-defined rotational character. However, the distribution of the modes are not identical; at liquid densities, the solvation response is clearly concentrated in the high-frequency portion of the spectrum (say, $\omega > 600$ cm^{-1}), while at lower densities, the distribution of frequencies presents a much broader profile. Furthermore, the subsequent decomposition of $D_s^R(\omega)$ from rotations around the three principal molecular axes shown in Figure 12 reveals that the major contribution to $D_s^R(\omega)$ comes from rotations around the molecular *y* axis (here chosen parallel to the H−H bond), while there is almost no contributions from projections into the *z* axis coinciding with the direction of the molecular dipole. The simple consideration of the magnitude of the moment of inertia I_y, which for the case of water is between two and three times smaller than the other two, can be invoked to account for the prevalence of the rotations around the *y* axis. On the other hand, the absence of a contribution from rotations around the *z* axis appears as a quite obvious result since, within the dipolar approximation, such rotations have no effects on the solute−solvent Coulomb coupling.

The comparison of the spectral areas provides a quantitative idea of the relative efficiency of rotational over translational mechanisms for solvation; in Table 2 we have also included results for f_s defined as

$$f_s = \frac{\int D_s^R(\omega)\, d\omega}{\int D_s^T(\omega)\, d\omega} \quad (36)$$

The areas of the supercritical rotational spectra are 100−200 times larger than the translational ones; the magnitude of these ratios should be compared to the result found in ref 66 for the solvation of a model dumbbell solute in liquid acetonitrile, which is 2 orders of magnitude smaller, $f_s \simeq 3$. The fact that for all practical purposes the solvation response of water is exclusively driven by rotational dynamics comes as a consequence of a more general result based on the characteristics of solute−solvent coupling V_c. Using symmetry arguments and invoking simple scaling laws, Ladanyi and Stratt[68] have demonstrated that for dipolar solvation, the following expression for f_s holds

$$f_s \propto \frac{M\langle r \rangle^2}{I} \quad (37)$$

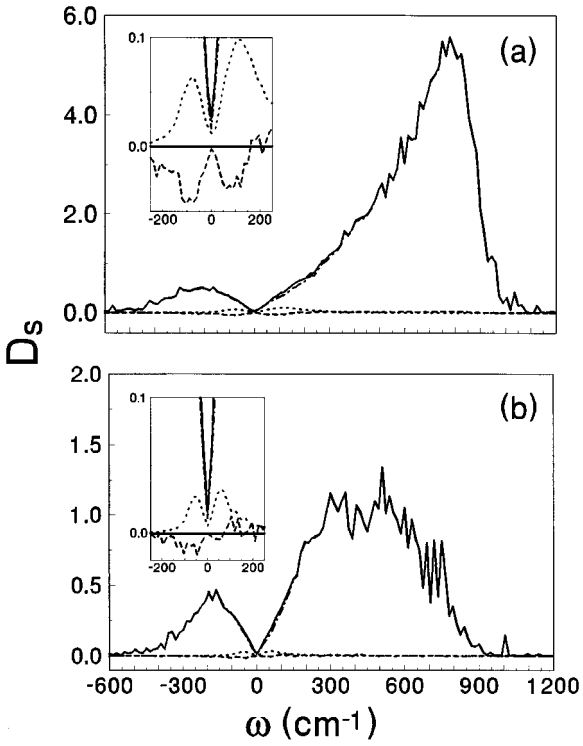

Figure 11. Solvation spectra (in units of 10^7 J^2 kg^{-1} m^{-2} cm) for supercritical water at different densities. (a) $\rho = 1$ g cm^{-3}; (b) $\rho = 0.3$ g cm^{-3}. D_s (solid line); D_s^T (dotted line); D_s^R (dashed−dotted line); D_s^C (dashed line).

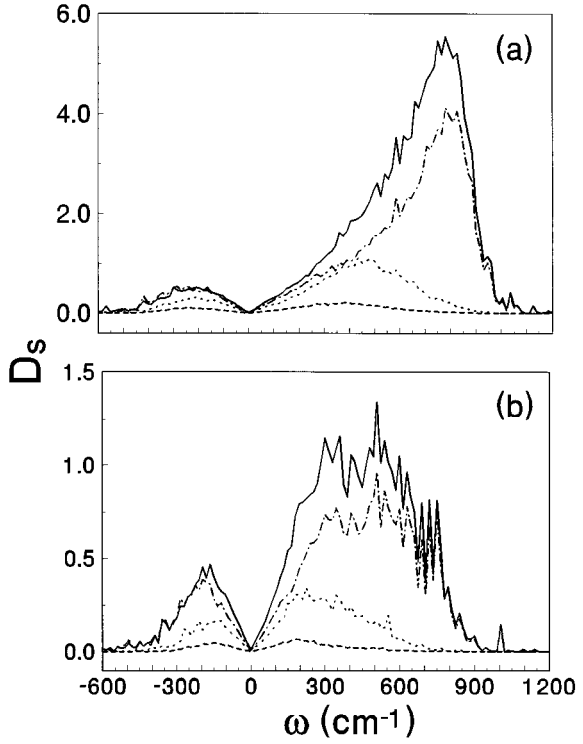

Figure 12. Contributions to D_s^R from rotations around different principal molecular axes (see text). (a) $\rho = 1$ g cm^{-3}; (b) $\rho = 0.3$ g cm^{-3}. D_s^R (solid line); *x* axis (dotted line); *y* axis (dashed−dotted line); *z* axis (dashed line). The cross contributions are not shown. Same units as Figure 11.

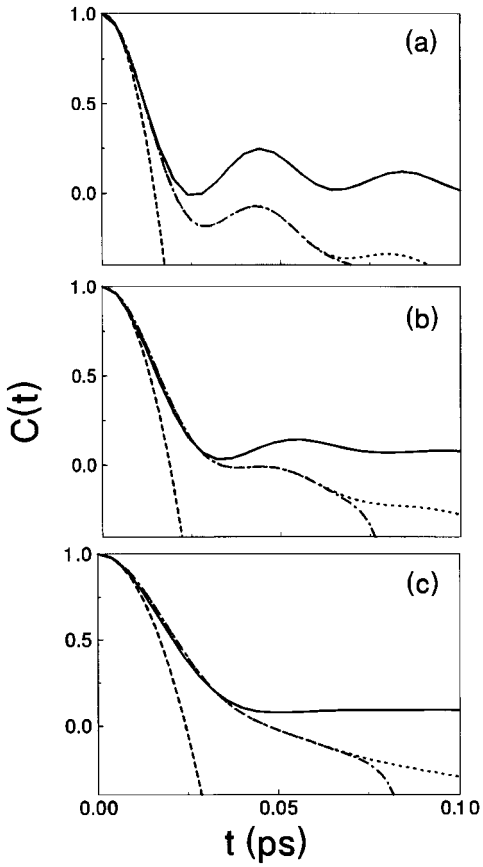

Figure 13. Equilibrium time correlation functions for the Coulomb portion of the solute−solvent coupling at different supercritical conditions. (a) $\rho = 1$ g cm^{-3}; (b) $\rho = 0.65$ g cm^{-3}; (c) $\rho = 0.3$ g cm^{-3}. Simulation results (solid line); INM results including imaginary frequencies (dashed−dotted lines); INM results excluding imaginary frequencies (dotted lines); Gaussian approximation using ω_s^{INM} from Table 2 (dashed lines).

where I represents the value for a representative momentum of inertia and $\langle r \rangle$ is a typical length scale characterizing interparticle interactions, here approximated by $\langle r \rangle \simeq \rho^{-1/3}$; from eq 37, we obtain for aqueous solvation, $f_s \simeq 200-600$. As a remarkable feature, we note that the relative rotational and translational contributions to the solvation response as reflected by the values of f_s not only satisfy the predicted density trend but are also comparable in order of magnitude to the estimates computed using eq 37.

To conclude, in Figure 13 we present results for $C(t)$ obtained using eq 28. The inclusion of the full frequency spectrum in the calculations leads to an exponential divergence of the correlation functions after 50−60 fs due to the presence of imaginary frequencies. Anyhow, the divergence does not represent a problem here since INM predictions for $C(t)$ remain in acceptable agreement with the molecular dynamics results only during the first 25−40 fs; although in principle this interval might look extremely brief, it is enough to cover in all cases more than 85% of the total relaxation of $C(t)$. As a final test of internal consistency of our calculations, in the last column of Table 2 we present values for the solvation frequency computed using the limit $t \rightarrow 0$ of the second derivative of eq 28, namely

$$\omega_s^{INM} = \frac{k_B T}{\langle (\delta V_c)^2 \rangle_{z_i=0}} \int D_s(\omega)\, d\omega \qquad (38)$$

As noted by Stratt and Cho,[65] the INM result for $C(t)$ is correct up to the t^4 term in the short time expansion of the exact correlation function; therefore, the agreement between ω_s^{INM} and the values obtained by the Gaussian fit of the actual $C(t)$ provides a clear confirmation of the quality of our results.

6. Concluding Remarks

In this study we have presented new results for the dynamical response of water at different supercritical conditions. In performing our simulation experiments, two main objectives were pursued: the first one was to determine the time scales that characterize the overall solvation process; second, we examined the basic mechanisms that drive the solvation in high-temperature aqueous solutions putting special emphasis in understanding how these mechanisms are related to the microscopic details of the particular structure of water at $T = 645$ K. At liquidlike densities, the overall solvation process is approximately 10 times faster than at room temperature; $S(t)$ involves only just a couple of underdamped oscillations, which die off beyond 100 fs. These differences are not to be found in the magnitude of the corresponding inertial frequencies, which for both cases are close to 100 ps^{-1}, but in the subsequent diffusional regime that is practically absent at this supercritical condition. At densities much closer to the critical one, the contributions from the fast rotational relaxations get reduced to approximately one-half of the total response, while the rest arises from a much slower diffusive stage representing the solvent aggregation around the newly generated ion.

We also found that predictions from linear response theories based on the equilibrium time correlation functions still provide adequate descriptions of the early inertial stage of solvation. The possibility of performing simulations at supercritical temperatures allowed us to test the validity of simple theories relating individual rotational motions and the solvation response in a variety of environments spanning from steam to liquidlike with well-differentiated spatial and dipolar correlations. Surprisingly, in all cases we found that theories based on continuum models where the different polarization is taken into account solely via the value of ϵ are adequate to predict reasonably well the values of the solvation frequencies; moreover, the consideration of a single parameter α_s, depending on simple properties of the solvent, seems to be enough to describe the complete time behavior of $C(t)$ in terms of orientational correlations of the individual molecules, even in cases where these correlations exhibit time decays quite dissimilar.

The simulation results were complemented by an INM analysis that allowed us not only to confirm by an independent route the distinctive features of the solvation dynamics but also to investigate the topography of the potential energy surface that dictates the dynamics of the solvent. At all densities, the solvation is exclusively driven by the identical mechanisms, namely, rotational motions that mostly involve fast librations around the molecular y axis. At high densities, the solvation spectrum $D_s^R(\omega)$ is concentrated in the high-frequency wing and attains its maximum at $\omega \simeq 800$ cm^{-1}. Considering the information provided by the participation ratios, the harmonic motions in that frequency range correspond to collective displacements of around 15 solvent molecules, a number similar to the constituents of the first solvation shell. This observation is consistent with previous results of the solvation spectrum of acetonitrile[67] where the projection of spectrum into the closest solvation shell was very close to the total $D_s^R(\omega)$. Results from the INM analysis were not only qualitative. From the total areas of the solvation spectra, not only have we obtained values of ω_s^{INM} in good agreement with the solvation frequencies obtained from the actual correlation functions but furthermore,

by appropriate Fourier transforms, we were able to reconstruct the simulated time correlation functions over time periods sufficiently long to almost cover the complete relaxation.

Direct verification of the trends presented in this work is surely called for, and we hope that, despite the difficulties imposed by the extreme conditions of temperatures and pressures, our results can be validated by real experimental measurements in the near future.

Acknowledgment. We are deeply indebted to R. Fernández-Prini for many insightful discussions on an early version of this work. The research of D.L. is partially supported by a grant from Fundación Antorchas of Argentina.

References and Notes

(1) Fernández-Prini, R.; Japas, M. L. *Chem. Soc. Rev.* **1994**, *23*, 155.

(2) For recent advances in technological processes involving supercritical fluids, see, for example: *Innovations in Supercritical Fluids, Science and Technology*; Hutchenson, K. W., Foster, N. R., Eds.; ACS Symposium Series 608; American Chemical Society: Washington, DC, 1995.

(3) McHugh, M. A.; Krukonis, V. J. *Supercritical Fluid Extraction: Principles and Practice*; Butterworth: Boston, MA, 1986.

(4) (a) Kim, S.; Johnston, K. P. In *Supercritical Fluids, Chemical and Engineering Principles and Applications*; Squires, T. G., Paulatis, M. E., Eds.; ACS Symposium Series 329; American Chemical Society; Washington, DC, 1987. (b) Kim, S.; Johnston, K. P. *Ind. Eng. Chem. Res.* **1987**, *26*, 1206. (c) Bennet, G. E.; Johnston, K. P. *J. Phys. Chem.* **1994**, *98*, 441.

(5) Peck, D. G.; Mehta, A. J.; Johnston, K. P. *J. Phys. Chem.* **1989**, *93*, 4297.

(6) Johnston, K. P.; Haynes, C. *AIChE J.* **1987**, *33*, 2017.

(7) Ekert, C. A.; Ziger, D. H.; Johnston, K. P.; Kim, S. *J. Phys. Chem.* **1986**, *90*, 2378.

(8) Carlier, C.; Randolph, T. W. *AIChE J.* **1993**, *39*, 876.

(9) (a) Postorino, M. A.; Tromp, R. H.; Ricci, M. A.; Soper, A. K.; Neilson, G. W. *Nature* **1993**, *366*, 668. (b) Tromp, R. H.; Postorino, P.; Neilson, G. W.; Ricci, M. A.; Soper, A. K. *J. Chem. Phys.* **1994**, *101*, 6210.

(10) Fois, E. S.; Sprik, M.; Parrinello, M. *Chem. Phys. Lett.* **1994**, *223*, 411.

(11) Frank, E. U.; Roth, K. *Discuss. Faraday Soc.* **1967**, *43*, 108.

(12) Hoffman, M. M.; Conradi, M. S. *J. Am. Chem. Soc.* **1997**, *119*, 3811.

(13) Mountain, R. D. *J. Chem. Phys.* **1989**, *90*, 1866.

(14) (a) Cummings, P. T.; Cochran, H. D.; Simonson, J. M.; Mesmer, R. E.; Karaborni, S. *J. Chem. Phys.* **1991**, *94*, 5606. (b) Cochran, H. D.; Cummings, P. T.; Karaborni, S. *Fluid Phase Equilib.* **1992**, *71*, 2.

(15) (a) Guissani, Y.; Guillot, B. *J. Chem. Phys.* **1993**, *98*, 8221. (b) Guillot, B.; Guissani, Y. *J. Chem. Phys.* **1993**, *99*, 8075.

(16) Kalinichev, A. G. *Ber. Bunsen-Ges. Phys. Chem.* **1993**, *97*, 872.

(17) Mizan, T. I.; Savage, P. E.; Ziff, R. M. *J. Phys. Chem.* **1994**, *98*, 13067.

(18) Martí, J.; Padro, J. A.; Guardià, E. *J. Chem. Phys.* **1996**, *105*, 639.

(19) (a) Jedlovsky, P.; Vallauri, R. *J. Phys. Chem.* **1996**, *105*, 2391. (b) Soper, A. K.; Bruni, F.; Ricci, M. A. *J. Chem. Phys.* **1997**, *106*, 247.

(20) For a comparative analysis of different model Hamiltonians, see: Chialvo, A. A.; Cummings, P. T. *J. Chem. Phys.* **1994**, *101*, 4426.

(21) Wood, R. H.; Quint, J. R.; Grolier, J.-P. E. *J. Chem. Phys.* **1981**, *85*, 3944.

(22) Luo, H.; Tucker, S. C. *J. Phys. Chem.* **1996**, *100*, 11165.

(23) Cui, S. T.; Harris, J. G. *J. Phys. Chem.* **1995**, *99*, 2900.

(24) (a) Balbuena, P. B.; Johnston, K. P.; Rossky, P. J. *J. Am. Chem. Soc.* **1994**, *116*, 2689. (b) Flanagin, L. W.; Balbuena, P. B.; Johnston, K. P.; Rossky, P. J. *J. Phys. Chem.* **1994**, *99*, 5196.

(25) (a) Hynes, J. T. In *Ultrafast Dynamics of Chemical Systems*; Simon, J. D., Ed.; Kluwer: Dordrecht, 1994. (b) Rossky, P. J.; Simon, J. D. *Nature* **1994**, *370*, 263.

(26) References 27−31 are comprehensive reviews of recent advances in solvation dynamics.

(27) Barbara, P. F.; Jarzeba, W. *Adv. Photochem.* **1990**, *15*, 1.

(28) (a) Bagchi, B. *Annu. Rev. Phys. Chem.* **1989**, *40*, 115. (b) Bagchi, B.; Chandra, A. *Adv. Chem. Phys.* **1991**, *80*, 1.

(29) Maroncelli, M. *J. Mol. Liq.* **1993**, *57*, 1.

(30) (a) Maroncelli, M.; Kumar, P. V.; Papazyan, A.; Horng, M. L.; Rosenthal, S. J.; Fleming, G. R. In *Ultrafast Reaction Dynamics and Solvent Effects*; Gaudel, Y., Rossky, P. J., Eds.; American Institute of Physics: New York, 1994.

(31) Stratt, R. M.; Maroncelli, M. *J. Phys. Chem.* **1996**, *100*, 12981.

(32) Jimenez, R.; Fleming G. R.; Kumar, P. V.; Maroncelli, M. *Nature* **1994**, *369*, 471.

(33) Karim, O. A.; Haymet, A. D. J.; Banet, M. J.; Simon, J. D. *J. Phys. Chem.* **1988**, *92*, 3391.

(34) Maroncelli, M.; Fleming, G. R.; *J. Chem. Phys.* **1988**, *89*, 5044.

(35) Bader, J.; Chandler, D. *Chem. Phys. Lett.* **1989**, *157*, 501.

(36) (a) Levy, R. M.; Kitchen, D. B.; Blair, J. T.; Krogh-Jespersen, K. *J. Phys. Chem.* **1990**, *93*, 4470. (b) Belhadj, M.; Kitchen, D. B.; Blair, J. T.; Krogh-Jespersen, K.; Levy, R. M. *J. Phys. Chem.* **1991**, *95*, 1082.

(37) Fonseca, T.; Ladanyi, B. M. *J. Phys. Chem.* **1991**, *95*, 2116.

(38) Carter, E. A.; Hynes, J. T. *J. Chem. Phys.* **1991**, *94*, 5961.

(39) Maroncelli, M. *J. Chem. Phys.* **1991**, *94*, 2048.

(40) Papazyan, A,; Maroncelli, M. *J. Chem. Phys.* **1991**, *95*, 9219.

(41) Ando, K.; Kato, S. *J. Chem. Phys.* **1991**, *95*, 5966.

(42) Neria, E.; Nitzan, A. *J. Chem. Phys.* **1992**, *96*, 5433.

(43) Perera, L.; Berkowitz, M. L. *J. Chem. Phys.* **1992**, *96*, 3092. Perera, L.; Berkowitz, M. L. *J. Chem. Phys.* **1992**, *97*, 5253.

(44) Maroncelli, M.; Kumar, V. P.; Papazyan, A. *J. Phys. Chem.* **1993**, *97*, 13.

(45) Papazyan, A.; Maroncelli, M. *J. Chem. Phys.* **1993**, *98*, 6431.

(46) Benjamin, I. *Chem. Phys.* **1993**, *180*, 287.

(47) Muino, P. L.; Callis, P. R. *J. Chem. Phys.* **1994**, *100*, 4093.

(48) Olender, R.; Nitzan, A. *J. Chem. Phys.* **1993**, *102*, 7180.

(49) Skaf, M. S.; Ladanyi, B. M. *J. Phys. Chem.* **1996**, *100*, 18258.

(50) Berendsen, H. J. C.; Postma, J. P. M.; Von Gunsteren, W. F.; Hermans, J. *Intermolecular Forces*; Reidel: Dordrecht, 1981.

(51) Pettit, B. M.; Rossky, P. J. *J. Chem. Phys.* **1986**, *84*, 5836.

(52) Nosé, S. *Mol. Phys.* **1984**, *52*, 255.

(53) de Pablo, J. J.; Prausnitz, J. M.; Strauch, H. J.; Cummings, P. T. *J. Chem. Phys.* **1990**, *93*, 7355.

(54) Allen, M. P.; Tildesley, D. J. *Computer Simulations of Liquids*; Clarendon Press: Oxford, 1987.

(55) Ryckaert, J.-P.; Ciccotti, G.; Berendsen, H. J. C. *J. Comput. Phys.* **1977**, *23*, 327.

(56) Chandler, D. *An Introduction to Modern Statistical Mechanics*; Oxford University Press: New York, 1987; Chapter 8.

(57) Some studies also make a distinction between the initial Gaussian and the librational regimes. See, for example, refs 49 and 66.

(58) Re, M.; Laria, D.; Fernández-Prini, R. *Chem. Phys. Lett.* **1996**, *250*, 25.

(59) Margulis, C.; Laria, D.; Fernández-Prini, R. *J. Chem. Soc., Faraday Trans.* **1996**, *92*, 2703.

(60) For interpretations of the fast oscillations in different contexts, see, for example: (a) Impey, R. W.; Madden, P. A.; McDonald, I. R. *Mol. Phys* **1982**, *46*, 513. (b) Neumann, M. *J. Chem. Phys.* **1986**, *85*, 1567. (c) Guillot, B. *J. Chem. Phys.* **1991**, *95*, 1543. (d) Bertolini, D.; Tani, A. *Mol. Phys.* **1992**, *75*, 1065.

(61) For water molecules, the computation of I_{eff} represents a weighted sum of the moments of inertia not coincident with the dipolar moment. See refs 30 and 44 for more details.

(62) For a review of the INM formalism applied to liquids, see: Stratt, R. M. *Acc. Chem. Res.* **1995**, *28*, 201.

(63) (a) Xu, B.-C.; Stratt, R. M. *J. Chem. Phys.* **1990**, *92*, 1923. (b) Adams, J. E.; Stratt, R. M. *J. Chem. Phys.* **1990**, *93*, 1332. (c) Adams, J. E.; Stratt, R. M. *J. Chem. Phys.* **1990**, *93*, 1632. (d) Wan, Y.; Stratt, R. M. *J. Chem. Phys.* **1994**, *100*, 5123.

(64) Buchner, M.; Ladanyi, B.; Stratt, R. M. *J. Chem. Phys* **1992**, *97*, 8522.

(65) Stratt, R. M.; Cho, M. *J. Chem. Phys.* **1994**, *100*, 6700.

(66) Cho, M.; Fleming, G. R.; Saito, S.; Ohmine, I.; Stratt, R. M. *J. Chem. Phys.* **1994**, *100*, 6672.

(67) Ladanyi, B.; Stratt, R. M. *J. Phys. Chem.* **1995**, *99*, 2502.

(68) Ladanyi, B.; Stratt, R. M. *J. Phys. Chem.* **1996**, *100*, 1266.

(69) Goodyear, G.; Larsen, R. E.; Stratt, R. M. *Phys. Rev. Lett.* **1996**, *76*, 243.

(70) Zwanzig, R. *J. Chem. Phys.* **1983**, *79*, 4507.

(71) For a related picture based on transitions between inherent structures in liquids, see: (a) Stillinger, F. H.; Weber, T. A. *Phys. Rev. A* **1983**, *28*, 2408. (b) Stillinger, F. H. *J. Chem. Phys.* **1983**, *88*, 7818. (c) LaViolette R.; Stillinger, F. H. *J. Chem. Phys.* **1985**, *83*, 4079.

(72) For a series of applications of normal-mode analysis to compute transport properties, see: (a) Seeley, G.; Keyes, T. *J. Chem. Phys.* **1989**, *91*, 5581. (b) Madan, B.; Keyes, T.; Seeley, G. *J. Chem. Phys.* **1990**, *92*, 7565. (c) Seeley, G.; Keyes, T.; Madan, B. *J. Chem. Phys.* **1991**, *94*, 6762. (d) Madan, B.; Keyes, T.; Seeley, G. *J. Chem. Phys.* **1991**, *95*, 3487. (e) Seeley, G.; Keyes, T.; Madan, B. *J. Phys. Chem.* **1992**, *96*, 4076.

(73) (a) Kalbfleisch, T. S.; Zeigler, L. D.; Keyes, T. *J. Chem. Phys.* **1996**, *105*, 7034. (b) For experimental information about reactions of CH_3I in supercritical Ar, see: Fan, R.; Kalbfleisch, T. S.; Ziegler, L. D. *J. Chem. Phys.* **1996**, *104*, 3886.